The role of viscoelasticity in the mechanical modelling of rubbers

Cite as: AIP Conference Proceedings **2113**, 180013 (2019); https://doi.org/10.1063/1.5112751
Published Online: 02 July 2019

C. M. Andrade, J. R. Barros, D. M. Neto, A. Ramalho, M. C. Oliveira, L. F. Menezes, and J. L. Alves

The Role of Viscoelasticity in the Mechanical Modelling of Rubbers

C.M. Andrade[1, a)] J.R. Barros[2, a)], D.M. Neto[1, b)], A. Ramalho[1, c)], M.C. Oliveira[1, c)], L.F. Menezes[1, c)] and J.L. Alves[2, d)]

[1]*CEMMPRE, Department of Mechanical Engineering, University of Coimbra*
Polo II, Rua Luís Reis Santos, Pinhal de Marrocos, 3030-788 Coimbra, Portugal
[2]*CMEMS, Microelectromechanical Systems Research Unit, University of Minho*
Campus de Azurém, 4800-058 Guimarães, Portugal

[a)] {carlos.andrade, joao.barros}@student.dem.uc.pt
[b)] Corresponding author: diogo.neto@dem.uc.pt
[c)] {amilcar.ramalho, marta.oliveira, luis.menezes}@dem.uc.pt
[d)] jlalves@dem.uminho.pt

Abstract. Bipolar plates (BPPs) are the main component in proton exchange membrane fuel cells. In the last years, different manufacturing processes have been proposed as alternative to the traditional graphite BPPs, including the manufacture of thin stamped BPPs using the rubber pad forming process. In this context, the numerical simulation of the forming process is used to optimize of the process parameters. Thus, in addition to the modelling of the elastoplastic behavior of the metallic sheet, it is also necessary to describe the hyper-viscoelastic behavior of the rubber pad. The main objective of this study is to evaluate the importance of the viscous effect on the global behavior of two different polyurethanes, since the modelling of the viscoelastic behavior is significantly more complex than the hyperelastic one. Uniaxial compression and stress relaxation tests are carried out both experimentally and numerically, considering three loading/unloading velocities. The hyperelastic behavior is described by the Mooney-Rivlin model, while the viscoelasticity is modelled by a series of Maxwell elements. The results show that the viscous effect can be neglected in the numerical modelling of the rubber pad forming, if the rubber hardness value is low.

INTRODUCTION

Increasing attention has been given to fuel cell technology in order to replace the internal combustion engines in transportation applications [1]. Since the bipolar plates (BPPs) are the primary component of the proton-exchange membrane fuel cells, comprising most of the cost, special attention must be given to the manufacturing process. Accordingly, the rubber pad forming has been adopted in the manufacturing of thin stamped BPPs [2]. Indeed, thin stamped BPPs are viewed as a promising alternative to the traditional graphite BPPs in proton-exchange membrane fuel cells [3]. However, the forming of ultra-thin BPPs is prone to several forming defects, such as springback, wrinkles, thinning and fracture [4].

The adoption of numerical simulation tools in the design and optimization of the forming processes allows reducing the product development time and the manufacturing costs. Nevertheless, the accuracy of the numerical solutions is strongly dependent on the numerical model adopted in the finite element simulation [5]. The simulation of the rubber pad forming requires the modelling of the mechanical behavior of the rubber material, which is both elastic and viscous. Although most of the hyperelastic material models are simple to apply and analyze, the modelling of the viscoelastic behavior is significantly more complex due to the rate-dependent response [6]. Moreover, note that the problem under analysis involves the deformation of the metallic sheet (elastoplastic behavior) through the frictional contact interaction with the rubber pad (hyper-viscoelastic behavior).

Proceedings of the 22nd International ESAFORM Conference on Material Forming
AIP Conf. Proc. 2113, 180013-1–180013-6; https://doi.org/10.1063/1.5112751
Published by AIP Publishing. 978-0-7354-1847-9/$30.00

The main objective of this study is to evaluate the importance of the viscous effect on the global mechanical behavior of the rubber pad during the forming process. The mechanical behavior of two different synthetic rubbers is analyzed, such that the hyperelastic behavior is described by the Mooney-Rivlin model, while the viscoelasticity is modelled by a series of Maxwell elements. Both stress relaxation tests and uniaxial compression tests are carried experimentally, using three levels of strain rate during the loading/unloading. The calibration of the material parameters is performed by the least square method, minimizing the difference between numerical and experimental stress values.

EXPERIMENTAL PROCEDURE AND CONSTITUTIVE MODEL

Regarding the experimental procedure, two different mechanical tests were adopted to characterize the hyper-viscoelastic behavior of the rubbers. They are: (i) loading/unloading uniaxial compression tests using three strain rate levels and (ii) stress relaxation tests. Two different polyurethane (PUR) rubbers are analyzed (Fig. 1(a)), which present different values of hardness, namely 70 and 95 Shore A, hereinafter called PUR70 and PUR95, respectively.

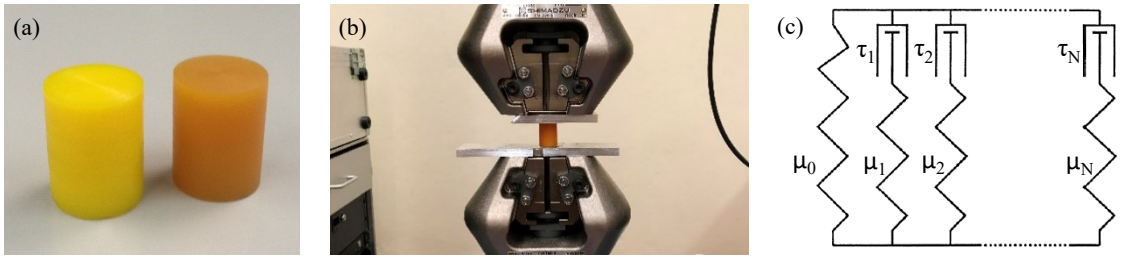

FIGURE 1. Experimental apparatus and constitutive model: (a) rubber specimens; (b) grips of the universal tensile testing machine; (c) generalized Maxwell model.

Uniaxial Compression and Stress Relaxation Tests

The experimental tests were performed on a Shimadzu universal tensile testing machine of maximum load 100 kN (Fig. 1(b)). The specimens used in the experiments are cylindrical with 25 mm of height and 18 mm of diameter (Fig. 1(a)), nominal dimensions in accordance with the study [7]. In order to reduce the friction between the rubber specimens and the flat compression plates (see Fig. 1(b)), glycerin was used on the contact interfaces. Hence, the uniaxial stress state is obtained in the uniaxial compression, avoiding the barreling effect. Each uniaxial compression test is composed by three stages: (i) loading; (ii) relaxation and (iii) unloading. Both the loading and the unloading are performed at the same grip velocity, but three different values of grip velocity are adopted, namely 0.05 mm/s, 0.5 mm/s and 5 mm/s, which leads three levels of strain rate (0.002 s^{-1}, 0.02 s^{-1} and 0.2 s^{-1}). The total prescribed displacement in the loading stage is 8.75 mm, which gives a stretch of 0.65 during the relaxation stage. Regarding the stress relaxation tests, the loading phase is performed with the largest grip velocity (5 mm/s) and the stretch (0.65) is kept constant for 10.000 seconds. The load and the crosshead displacement are recorded during the tests, allowing to evaluate the stress and the stretch evolution, respectively.

Hyper-Viscoelastic Constitutive Model

Since the rubbers are considered incompressible or nearly incompressible (Poisson's ratio tends to 0.5), the bulk modulus tends to infinity, which leads to null displacement solutions (volumetric locking) using the standard displacement finite element formulation. Therefore, a mixed u/P formulation is required to evaluate the mechanical behavior of rubber-like materials, where both the nodal displacements and the pressure are independent variables. In the present study, both PURs are considered nearly incompressible, with a ratio K/G of 1000, where K is the bulk modulus and G the shear modulus.

Rubber-like materials present a non-linear elastic stress-strain relation for large values of deformation. Therefore, they are usually described by constitutive models based on a strain energy density function, which can be defined by three parts: total deviatoric strain energy $\bar{W}(\bar{\mathbf{C}})$, volumetric strain energy $\bar{W}_{\mathrm{H}}(J)$ and the pressure balance that couples the mixed formulation, $Q^0(J)$, such as:

$$W(\mathbf{C}) = \bar{W}(\bar{\mathbf{C}}) + \bar{W}_{\mathrm{H}}(J) + Q^0(J) = \bar{W}(\bar{\mathbf{C}}) + \frac{K}{2}(J-1)^2 - \frac{1}{2K}(\bar{p} - \tilde{\ }\ , \tag{1}$$

where J is the Jacobian of the deformation gradient tensor, $\bar{p}$ is the pressure computed from the displacement field and $\tilde{\ }$ is the interpolated pressure from the pressure field (degree of freedom associated with the u/P method).

Considering the two parameter Mooney-Rivlin model, the deviatoric strain energy density is given by:

$$\bar{W}_{\mathrm{MR}}(\bar{\mathbf{C}}) = C_{10}(\bar{I}_1 - 3) + C_{01}(\bar{I}_2 - 3)\,, \tag{2}$$

where C_{10} and C_{01} are material parameters, while $\bar{I}_1$ and $\bar{I}_2$ denote the invariants of the deviatoric right Cauchy-Green deformation tensor $\bar{\mathbf{C}}$, which can be described as a function of the principal stretches λ_1, λ_2 and λ_3 by:

$$\bar{I}_1 = J^{-\frac{2}{3}} I_1 = J^{-\frac{2}{3}}(\lambda_1^{\,2} + \lambda_2^{\,2} + \lambda_3^{\,2})\,, \tag{3}$$

$$\bar{I}_2 = J^{-\frac{4}{3}} I_2 = J^{-\frac{4}{3}}(\lambda_1^{\,2}\lambda_2^{\,2} + \lambda_2^{\,2}\lambda_3^{\,2} + \lambda_3^{\,2}\lambda_1^{\,2})\,. \tag{4}$$

According to the Mooney-Rivlin strain energy density and assuming material incompressibility (J=1), the first Piola-Kirchhoff stress for the uniaxial stress state ($\lambda_1 = \lambda$ and $\lambda_2 = \lambda_3 = 1/\sqrt{\lambda}$) is be obtained by:

$$PK1_{\mathrm{MR}} = \frac{\partial \bar{W}_{\mathrm{MR}}(\lambda)}{\partial \lambda} = 2(1 - \lambda^{-3})(C_{10}\lambda + C_{01})\,. \tag{5}$$

In addition to the non-linear stress-strain behavior, rubber-like materials are usually strain-rate sensitive (viscous effect). This hyper-viscoelastic behavior can be represented by a rheological analogy – the generalized Maxwell model (Fig. 1(c)). This model is defined by an elastic spring (hyperelastic behavior) in parallel with m Maxwell elements (visco elasticity), where each Maxwell element is composed by an elastic spring and a viscous Newton-element in series. Accordingly, the second Piola-Kirchhoff stress for the uniaxial stress state is given by:

$$\prod_{\mathrm{Total}} = \prod_{\mathrm{MR}} + \sum_{i=1}^{m} \prod_{\mathrm{MW}_i}\,, \tag{6}$$

where $\prod_{\mathrm{MR}}$ denotes the second Piola-Kirchhoff stress derived from the Mooney-Rivlin strain energy density (hyperelastic behaviour) and $\prod_{\mathrm{MW}_i}$ is the second Piola-Kirchhoff stress generated by i^{th} Maxwell element. Since the response of each Maxwell element depends on the hyperelastic behavior (time-independent) given by the Mooney-Rivlin strain energy density, the second Piola-Kirchhoff stress in each Maxwell element must be evaluated incrementally. Hence, the stress in the i^{th} Maxwell element at the increment n+1 is given by:

$$\prod_{\mathrm{MW}_i}{}^{n+1} = \exp\left(-\frac{\Delta t}{\tau_i}\right)\prod_{\mathrm{MW}_i}{}^{n} + \frac{ak_i\tau_i}{\Delta t}\left[1 - \exp\left(-\frac{\Delta t}{\tau_i}\right)\right]\left(\prod_{\mathrm{MR}}{}^{n+1} - \prod_{\mathrm{MR}}{}^{n}\right), \tag{7}$$

where Δt is the time increment, while τ_i and ak_i are parameters related to the i^{th} Maxwell element. For each Maxwell element, the dashpot relaxation time is denoted by τ_i and $ak_i = \mu_i/\mu_0$ is the ratio between the constant of the Maxwell elastic spring and the time-independent elastic part of the deformation (see Fig. 1 (c)).

CALIBRATION OF MATERIAL PARAMETERS

For each PUR under analysis, the material parameters involved in the hyper-viscoelastic/hyperelastic constitutive model were evaluated using data from the experimental tests: (i) loading/relaxation/unloading uniaxial compression tests and (ii) stress relaxation tests. The numerical simulations of these tests were carried out using the in-house finite element code V-Biomech, which was originally developed to analyze musculo-skeletal systems and soft tissues [8]. The nonlinear least square fitting was adopted to calibrate the material parameters, comparing the experimental and the numerical first Piola-Kirchhoff stress evolutions. In addition to the relaxation test, regarding the loading/relaxation/unloading uniaxial compression tests, three different values of grip velocity (0.05 mm/s, 0.5 mm/s and 5 mm/s) are considered simultaneously in the curve fitting. Thus, the least square method is defined by:

$$LSM = \min \sum_{i=1}^{k} (PK1_{\mathrm{exp}}^{i} - PK1_{\mathrm{num}}^{i})^2\,, \tag{8}$$

where the subscripts "exp" and "num" denote the experimental and numerical data, respectively. In order to give equal weight for all tests, the same number of points was used to define each of the four curves, corresponding to each test. Moreover, the loading and the unloading stages are also defined by the same number of points.

TABLE 1. Material parameters obtained by curve fitting for each PUR studied, considering both hyper-viscoelastic and only hyperelastic behavior.

	C_{10}	C_{01}	ak_1	ak_2	τ_1	τ_2
PUR70 Hyper-viscoelastic model	1.195	0.000	0.0962	0.0717	781.7	9.09
PUR70 Hyperelastic model	1.316	0.000	-	-	-	-
PUR95 Hyper-viscoelastic model	3.523	0.000	0.1765	1.0939	16.46	0.117
PUR95 Hyperelastic model	3.777	0.000	-	-	-	-

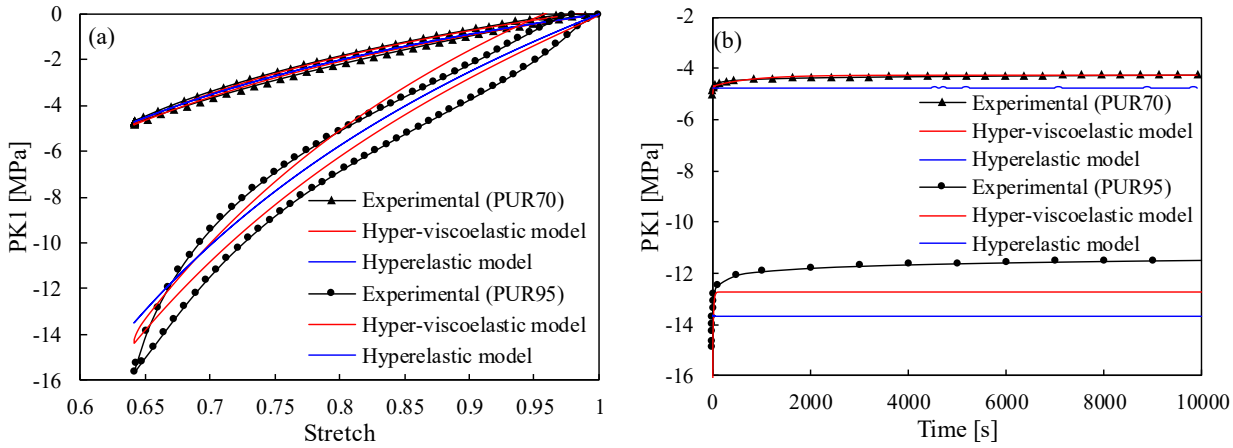

FIGURE 2. Comparison between the experimental and numerical first Piola-Kirchhoff stress for both PURs: (a) loading/relaxation/unloading uniaxial compression tests at 0.5 mm/s grip velocity; (b) stress relaxation tests. Two different constitutive models are considered in the numerical model, considering both hyper-viscoelastic and only hyperelastic behavior.

For each PUR analyzed in this study, the curve fitting was carried out considering: (i) only the parameters of the hyperelastic model and (ii) the parameters of the hyper-viscoelastic model. The obtained parameters are listed in Table 1 for each material (PUR70 and PUR95) and for both constitutive models. The comparison between experimental and predicted first Piola-Kirchhoff stress is presented in Fig. 2 for both materials, considering both constitutive models previously presented. The loading/unloading of the uniaxial compression tests at 0.5 mm/s grip velocity are shown in Fig. 2 (a), highlighting the influence of the rubber hardness on the attained stress values. Moreover, the largest difference between the loading and unloading curve occurs in the PUR95, i.e. the viscous effect is more pronounced for this material. Thus, the adoption of a hyper-viscoelastic constitutive model significantly improves the mechanical behavior modelling, as shown in Fig. 2 (a). The stress relaxation tests are presented in Fig. 2 (b), where the time-independent constitutive model (hyperelastic behavior) leads to a constant stress value for a fixed value of stretch. On the other hand, an improved prediction of the stress relaxation is obtained using the hyper-viscoelastic constitutive model, particularly for the PUR70. Nevertheless, considering the PUR95, the experimental stress relaxation is underestimated by the numerical model, which presents a substantial stress relaxation in the first 50 seconds followed by a stable value. This is a consequence of the calibrated material parameters, specifically the relaxation time of each dashpot defining the Maxwell elements, which present low order values (see Table 1).

STRAIN PATHS IN RUBBER PAD FORMING PROCESSES

In order to find the strain paths arising in the rubber pad forming operation, a finite element model of the forming process was developed in Abaqus [9]. The forming process is composed by: a fixed lower rigid die with the geometry of the flow channels present in the BPPs; the thin metallic sheet comprising isotropic elastoplastic behaviour; and the rubber pad on which the prescribed displacement is applied. The contact with friction was considered in all contact interfaces, using a constant friction coefficient of 0.1. Considering the material parameters listed in Table 1 for the PUR70 defined by the hyper-viscoelastic model, the different stress states in the rubber pad are schematic identification in Fig. 3, ranging from uniaxial compression to uniaxial tension.

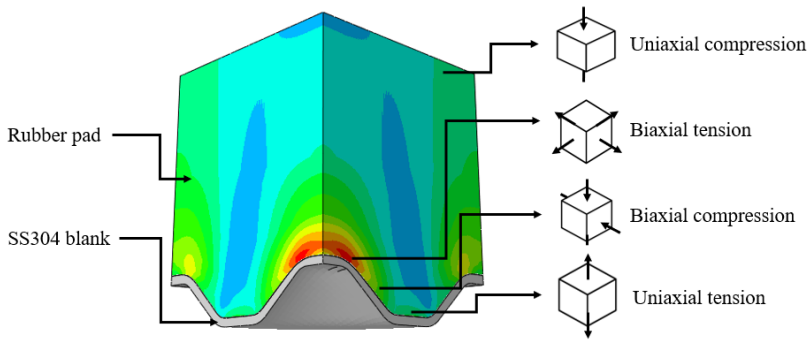

FIGURE 3. Schematic identification of the stress states arising in the rubber pad during the forming operation.

Thus, the accurate mechanical characterization of a rubber material behavior requires experimental data from different mechanical tests (tensile, compression, shear, biaxial, etc.). However, some of these tests are difficult to carried out, requiring dedicated equipment and specimens with complex geometry. Moreover, it is also important to define how important it will be to perform these tests for different strain rate levels. Thus, although the calibration of the material parameters was previously performed using only uniaxial compression tests, the mechanical behavior of the rubbers (PUR70 and PUR95) was evaluated numerically considering different strain paths.

A unitary finite element model was created in V-Biomech to study the rubber behavior in different mechanical tests, namely the equi-biaxial tension test ($\lambda_1 = \lambda_2 = \lambda$ and $\lambda_3 = \lambda^{-2}$), the planar tensile test ($\lambda_1 = \lambda$, $\lambda_2 = \lambda^{-1}$ and $\lambda_3 = 1$) and the uniaxial tension test ($\lambda_1 = \lambda$ and $\lambda_2 = \lambda_3 = \lambda^{-1/2}$). The numerical simulations were performed using the material parameters listed in Table 1, i.e. enabling the comparison of the hyperelastic and the hyper-viscoelastic constitutive models, for each test. Since the hyper-viscoelastic behavior is time-dependent, a strain rate of 0.02 s^{-1} was adopted in all tests. Fig. 4 presents the first Piola-Kirchhoff stress evolution with the stretch for the three strain paths under analysis, highlighting the viscous effect for each PUR. The difference between the mechanical behavior described by the hyperelastic and the hyper-viscoelastic constitutive model shows that the PUR70 is less time-sensitive. Indeed, the stress values are lower at the end of the loading considering the viscous effect in the modeling of the PUR95, as shown in Fig. 4 (b).

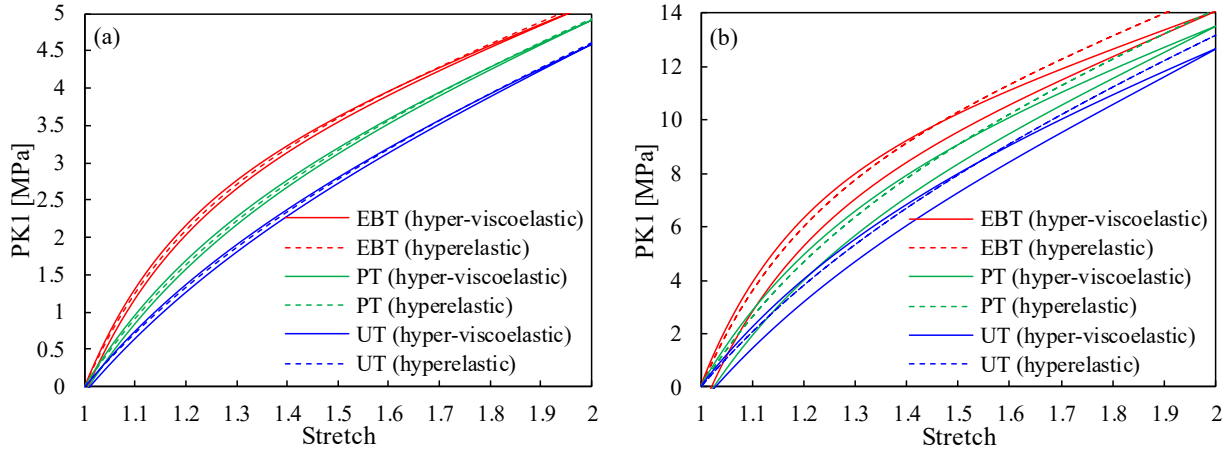

FIGURE 4. Numerical prediction of the first Piola-Kirchhoff stress evolution under different strain paths: (a) PUR70; (b) PUR95. EBT: Equi-Biaxial Tension test; PT: Planar Tensile test; UT: Uniaxial Tensile test.

CONCLUSIONS

This study presents the mechanical characterization of two polyurethane (PUR) rubbers with different hardness values (ShA70 and ShA95). In order to evaluate the importance of the viscous effect on the global mechanical behavior, both materials were modeled by a hyperelastic and a hyper-viscoelastic constitutive model. The hyperelastic behavior was modelled by the Mooney-Rivlin strain energy density, while the viscoelasticity was modelled by a series

of Maxwell elements. Both stress relaxation tests and uniaxial compression tests were carried out experimentally, using three different strain rates during the loading/unloading of the uniaxial compression tests. Then, the least squares method was adopted in the calibration of the material parameters, obtaining two sets of material parameters for each PUR, which corresponds to the inclusion or not of the viscous effect. The results shown that the adoption of the hyper-viscoelastic model improves the prediction accuracy. Nevertheless, the experimental loading/unloading shows that the viscous effect is more significant in the PUR presenting the higher hardness value. Since different strain paths arise in the rubber pad during the forming operation of bipolar plates, a finite element model was created in V-Biomech to study three different mechanical tests: equi-biaxial tension, planar tension and uniaxial tension. Despite no experimental data is available for comparison, the stress-strain curves show the general expected behavior for rubber-like materials, i.e. the stress is higher in the equi-biaxial tension, followed by the planar tension and uniaxial tension.

ACKNOWLEDGMENTS

The authors gratefully acknowledge the financial support of the Portuguese Foundation for Science and Technology (FCT) under the projects with reference PTDC/EMS-TEC/0702/2014 (POCI-01-0145-FEDER-016779) and PTDC/EMS-TEC/6400/2014 (POCI-01-0145-FEDER-016876) by UE/FEDER through the program COMPETE2020 under the project MATIS (CENTRO-01-0145-FEDER-000014).

REFERENCES

1. Y. Wang, K. S. Chen, J. Mishler, S. C. Cho, and X. C. Adroher, *A review of polymer electrolyte membrane fuel cells: Technology, applications, and needs on fundamental research*, Appl. Energy **88**, 981–1007 (2011).
2. Y. Liu and L. Hua, *Fabrication of metallic bipolar plate for proton exchange membrane fuel cells by rubber pad forming*, J. Power Sources **195**, 3529–3535 (2010).
3. H. Wang and J. A. Turner, *Reviewing Metallic PEMFC Bipolar Plates*, Fuel Cells **10**, 510–519 (2010).
4. W. T. Park, C. K. Jin, and C. G. Kang, *Improving channel depth of stainless steel bipolar plate in fuel cell using process parameters of stamping*, Int. J. Adv. Manuf. Technol. **87**, 1677–1684 (2016).
5. W. Charon, M.-C. Iltchev, and J.-F. Blachot, *Mechanical simulation of a Proton Exchange Membrane Fuel Cell stack using representative elementary volumes of stamped metallic bipolar plates*, Int. J. Hydrogen Energy **39**, 13195–13205 (2014).
6. M. Kaliske, L. Nasdala, and H. Rothert, *On damage modelling for elastic and viscoelastic materials at large strain*, Comput. Struct. **79**, 2133–2141 (2001).
7. A. Vandenbroucke, H. Laurent, N. A. Hocine, and G. Rio, *A Hyperelasto-Visco-Hysteresis model for an elastomeric behaviour : Experimental and numerical investigations*, Comput. Mater. Sci. **48**, 495–503 (2010).
8. J. L. Alves, N. Yamamura, T. Oda, and C. Teodosiu, "Numerical simulation of musculo-skeletal systems by V-Biomech," in *9th International Symposium Computer Methods in Biomechanics and Biomedical Enginnering*, (2010).
9. Abaqus, "Theory Manual", version 6.11, (2016).